Development of cyclic peptides with potent in vivo osteogenic activity through RaPID-based affinity maturation

Nasir K. Bashiruddin[a], Mikihito Hayashi[b,c], Masanobu Nagano[a], Yan Wu[a], Yukiko Matsunaga[d], Junichi Takagi[d], Tomoki Nakashima[b,e,1], and Hiroaki Suga[a,1]

[a]Department of Chemistry, Graduate School of Science, The University of Tokyo, Tokyo 113-0033 Japan; [b]Department of Cell Signaling, Graduate School of Medical and Dental Sciences, Tokyo Medical and Dental University, Tokyo 113-8549, Japan; [c]Japan Agency for Medical Research and Development, Precursory Research for Innovative Medical Care, Tokyo 113-8549, Japan; [d]Laboratory of Protein Synthesis and Expression, Institute for Protein Research, Osaka University, Suita-shi, Osaka 565-0871, Japan; and [e]Japan Agency for Medical Research and Development, Core Research for Evolutional Science and Technology, Tokyo 113-8549, Japan

Edited by Laura L. Kiessling, Massachusetts Institute of Technology, Cambridge, MA, and approved October 13, 2020 (received for review June 16, 2020)

Osteoporosis is caused by a disequilibrium between bone resorption and bone formation. Therapeutics for osteoporosis can be divided into antiresorptives that suppress bone resorption and anabolics which increase bone formation. Currently, the only anabolic treatment options are parathyroid hormone mimetics or an anti-sclerostin monoclonal antibody. With the current global increases in demographics at risk for osteoporosis, development of therapeutics that elicit anabolic activity through alternative mechanisms is imperative. Blockade of the PlexinB1 and Semaphorin4D interaction on osteoblasts has been shown to be a promising mechanism to increase bone formation. Here we report the discovery of cyclic peptides by a novel RaPID (Random nonstandard Peptides Integrated Discovery) system-based affinity maturation methodology that generated the peptide PB1m6A9 which binds with high affinity to both human and mouse PlexinB1. The chemically dimerized peptide, PB1*d*6A9, showed potent inhibition of PlexinB1 signaling in mouse primary osteoblast cultures, resulting in significant enhancement of bone formation even compared to non-Semaphorin4D–treated controls. This high anabolic activity was also observed in vivo when the lipidated PB1*d*6A9 (PB1*d*6A9-Pal) was intravenously administered once weekly to ovariectomized mice, leading to complete rescue of bone loss. The potent osteogenic properties of this peptide shows great promise as an addition to the current anabolic treatment options for bone diseases such as osteoporosis.

PlexinB1 | cyclic peptides | osteoporosis | in vitro selection

Osteoporosis is a common cause of bone fracture in the elderly, costing billions globally due to fractures leading to long-term disability and subsequent exit from the working population (1, 2). Several treatment options are available for osteoporosis which can be divided into antiresorptives and anabolics ranging from orally dosed small molecules to injectable peptides and biologics (2, 3). Antiresorptive and anabolic agents differ in that antiresorptives inhibit or reduce bone resorption, thereby suppressing bone remodeling, whereas anabolics enhance the rate of bone formation while allowing continued resorption and remodeling of bone tissue. Although both treatments result in increased bone mass, resorption and remodeling are key to the microstructural integrity of bone, and emerging evidence points toward anabolics being more effective in reducing fracture (4–6). Currently, the only anabolics in the clinic are the parathyroid hormone and parathyroid hormone-related peptide mimetics (teriparatide and abaloparatide, respectively) and the sclerostin inhibitor monoclonal antibody (romosozumab). Teriparatide and abaloparatide both cannot be administered over 24 mo in a patient's lifetime due to the risk for developing osteosarcomas, and romosozumab treatment is recommended for 12 mo due to waning efficacy beyond this duration (7, 8). Therefore, with the ever increasing global median age and associated osteoporosis cases, the development of additional anabolic treatment options are of high importance.

Bone resorption and bone formation are regulated through communications between osteoclasts and osteoblasts, respectively (9). Among the paracrine factors involved in this process, axon guidance molecules, such as Semaphorin4D (Sema4D) and Semaphorin3A, mediate the regulation of bone cell differentiation. Sema4D, which is expressed and secreted by mature osteoclasts, inhibits osteoblast differentiation through its receptor PlexinB1 (PlxnB1) expressed on osteoblast surfaces. Binding of Sema4D to PlxnB1 leads to the inhibition of the activation of insulin receptor substrate-1 which is downstream of insulin-like growth factor-1 signaling. In addition, Sema4D controls the spatial distribution of bone-forming osteoblasts through PlxnB1-RhoA signaling (10). Mice with genetic deletion of Sema4D or PlxnB1 as well as mice expressing a dominant-negative form of RhoA in osteoblasts exhibit a high bone mass phenotype due to increased bone formation (11). These findings suggest that inhibiting PlxnB1-Sema4D signaling would lead to a bone

Significance

Osteoporosis affects over 75 million people globally, and this number is increasing with global median age. Therefore, the development of therapeutics with novel mechanisms of action is of high importance. Inhibition of the PlexinB1-Semaphorin4D interaction on osteoblasts has been shown to be a potential target for developing osteoanabolic modalities. Here, using a novel affinity maturation approach for cyclic peptides, we were able to develop cyclic peptide that tightly binds human and mouse PlexinB1 and inhibits its interaction with Semaphorin4D. Chemical dimerization of this peptide resulted in further increases in activity and demonstrated complete rescue of bone loss in an osteoporosis mouse model.

Author contributions: N.K.B., J.T., T.N., and H.S. designed research; N.K.B., M.H., M.N., Y.W., Y.M., and H.S. performed research; N.K.B., M.H., M.N., Y.M., J.T., T.N., and H.S. contributed new reagents/analytic tools; N.K.B., M.H., M.N., Y.W., Y.M., J.T., T.N., and H.S. analyzed data; and N.K.B., M.H., Y.W., J.T., and H.S. wrote the paper.

Competing interest statement: N.K.B., Y.M., J.T., and H.S. are inventors of a patent application titled "Plexin Binding Regulator" (US20190247457A1). All other authors declare no competing interests.

This article is a PNAS Direct Submission.

[1]To whom correspondence may be addressed. Email: naka.csi@tmd.ac.jp or hsuga@chem.s.u-tokyo.ac.jp.

This article contains supporting information online at https://www.pnas.org/lookup/suppl/doi:10.1073/pnas.2012266117/-/DCSupplemental.

First published November 23, 2020.

anabolic effect through enhancement of osteoblastic differentiation while keeping osteoblasts away from osteoclasts to enable efficient osteoclastic bone resorption.

We have previously reported a macrocyclic peptide discovery campaign to identify binding sites on PlxnB1 that inhibit its interaction with Sema4D by means of messenger RNA (mRNA) display in combination with genetic code reprogramming, referred to as the RaPID (Random nonstandard Peptides Integrated Discovery) system (12). We successfully identified a 16-mer thioether-macrocyclic peptide, PB1m6, capable of binding human PlxnB1 (hPlxnB1) with single-digit nanomolar-binding affinity and inhibiting its interaction with Sema4D (13). X-ray structural analysis of cocrystals of PB1m6 and hPlxnB1 revealed that PB1m6 is a negative allosteric modulator of the hPlxnB1-Sema4D interaction by binding a cleft distal to the Sema4D-binding interface of hPlxnB1 while still able to inhibit the hPlxnB1-Sema4D interaction. However, PB1m6 was shown to be selective toward hPlxnB1 over mouse PlxnB1 (mPlxnB1) displaying no detectable affinity (dissociation constant (K_D) over 1 μM) regardless of having 88% sequence identity in the N-terminal sema domains of hPlxnB1 and mPlxnB1. Modeling efforts based on the three-dimensional (3D) structure to rationally increase the species cross-reactivity were unsuccessful in our hands. This high selectivity is often observed with RaPID-derived macrocyclic peptides and is generally considered beneficial (13–18). However, in this instance, the high selectivity of PB1m6 hinders its ability to validate the inhibitory mechanism in mouse models. In this study, we used a fragmented saturation mutagenesis approach to create an mRNA library of PB1m6 analogs to be utilized in a RaPID selection campaign against mouse PlxnB1. After five iterative rounds of selection, we discovered a PB1m6 analog, referred to as PB1m6A9, exhibiting enhanced cross-reactivity with 44 nM K_D against mouse PlxnB1 and which, remarkably, also showed 10-fold stronger binding affinity against human PlxnB1 (0.28 nM K_D). To further improve apparent affinity and inhibitory activity, a homodimer of PB1m6A9 was chemically synthesized (PB1*d*6A9), and it was shown to exhibit potent mPlxnB1-Sema4D inhibitory activity in mouse primary osteoblasts as well as enhanced osteogenesis even when compared to cells not treated with Sema4D. Moreover, once-weekly intravenous (i.v.) administration of palmitoylated PB1*d*6A9 (PB1*d*6A9-Pal) in a mouse model of postmenopausal osteoporosis showed significant enhancement of bone formation compared to both vehicle and sham-operated (Sham) control mice. This work presents the facile development of a novel bone anabolic modality which shows promise as an addition to the current repertoire of anabolic agents used to address osteoporosis.

Results

Library Design for RaPID-Based Affinity Maturation and Selection for PB1m6 Analogs. Previous selection efforts discovered the peptide PB1m6 which binds PlxnB1 and was able to allosterically inhibit its interaction with Sema4D (13). However, PB1m6 was specific for human PlxnB1 and was not able to bind mouse PlxnB1 although they share 88% sequence identity in the PB1m6-binding region. Rational design efforts were not able to produce a cross-reactive analog peptide that can bind both human and mouse PlxnB1 in our hands. Therefore, we chose to take advantage of the high diversity of the RaPID system (>1 trillion peptides per selection) to generate a library where roughly half of the PB1m6 sequence is randomized to allow enough freedom to tweak its binding mode yet retain its "identity" to the original sequence so resultant peptides would be able to bind both human and mouse PlxnB1 at the same site. In addition, mutating several codons simultaneously can give rise to synergistic mutations which may not reveal themselves through such methods as deep mutational scanning where only single codons are investigated at a time (19). Several options are available for designing a library for the mutagenesis of an existing sequence such as error-prone PCR, doped oligonucleotide mutagenesis, and saturation mutagenesis (19–21). Error-prone PCR is often used in the directed evolution of enzymes. However, it is not able to generate our desired degree of mutagenesis. While a high degree of mutagenesis can be achieved with doped oligonucleotide mutagenesis, it cannot be as precisely controlled as saturation mutagenesis and results in the formation of completely random sequences when applied to the entire peptide sequence, and these unwanted non-PB1m6–like sequences may enrich during the selection process.

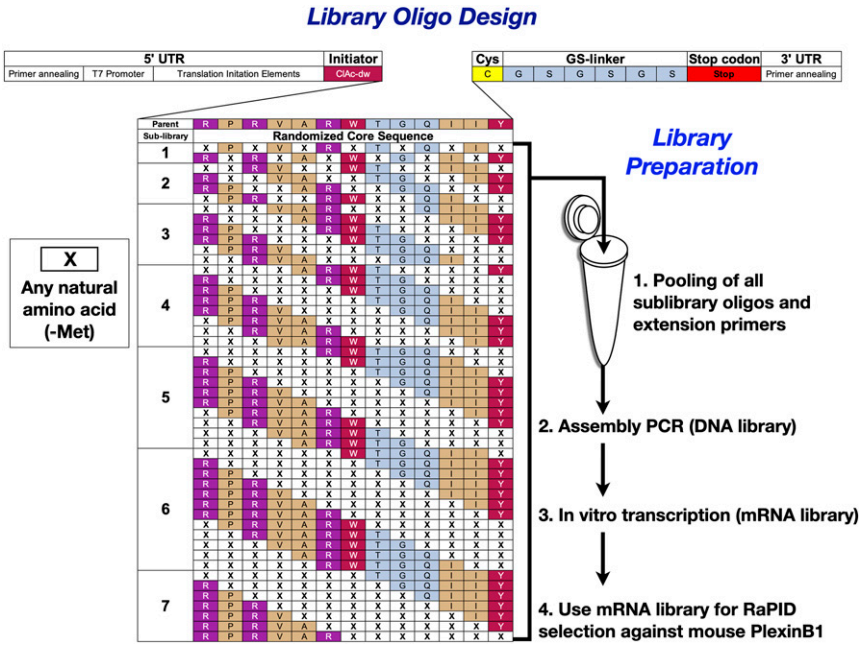

Fig. 1. Library design and preparation scheme for fragmented saturation mutagenesis of PB1m6.

Considering the merits and demerits of the above strategies, we decided to construct our library using a fragmented saturation mutagenesis approach where 49 sublibraries were pooled together, where each sublibrary encodes the PB1m6 peptide interspersed with NNK (N = A, T, G or C; K = T or G) codons (Fig. 1 and *SI Appendix*, Table S1). Each sublibrary was designed where NNK codons were distributed in groups of one to seven and alternating with a corresponding number of nonmutated codons, with the exception of the first amino acid (*N*-chloroacetyl–D-tryptophan) and the 15th amino acid (cysteine). With this fragmented saturation mutagenesis pattern, anywhere from 5 to 8 amino acids out of the 13 amino acid "core" were mutated in each sublibrary. When ignoring the sequence overlaps between sublibraries, the total theoretical sequence diversity is $\sim 10^{11}$, and while this is by no means an exhaustive sampling of all possible variations to the original sequence, we felt this was a sufficient compromise between sequence variation and the maximum diversity of the selection system ($>10^{12}$).

To physically construct the mRNA library, a DNA primer for each of the 49 sublibraries was synthesized and pooled followed by assembly PCR to add the 5′ and 3′ elements necessary for in vitro transcription and selection using the RaPID system. Following T7-mediated in vitro transcription, the mRNA library was used to select against an enzymatically biotinylated sema domain of mouse PlxnB1. In accordance with the original selection that produced PB1m6, the natural codon table was reprogrammed via Flexizyme with *N*-chloroacetyl–D-tryptophan in place of the initiator methionine to in vitro translate the library of PB1m6 analogs. Five iterative rounds of selection resulted in a 700-fold increase of mouse PlxnB1 binders (0.44% recovery) compared to the second selection round (0.0006% recovery) (*SI Appendix*, Fig. S1). In contrast, the recovery of nonspecific binders remained relatively constant across rounds 2–5, suggesting that specific enrichment of mPlxnB1-binding macrocyclic peptides had been achieved. Sequencing of the recovered round 5 pool revealed various PB1m6 analogs which were then chemically synthesized to confirm binding to mPlxnB1 (Fig. 2*A* and *SI Appendix*, Fig. S2). Indeed, surface plasmon resonance (SPR) analyses of the top five PB1m6 analogs all showed lower dissociation constants (K_D below 500 nM) to mPlxnB1 than the parental PB1m6 peptide. Notably, the analog PB1m6A9 exhibited the strongest binding affinity, with a K_D of 44 nM. Surprisingly, when assayed against human PlxnB1, PB1m6A9 showed over 10-fold improvement in binding affinity, with a K_D of 0.28 nM, while the parent peptide, PB1m6, has a K_D of 2.8 nM.

PB1m6A9 contains six mutated residues (R4Y, V5I, A6E, Q11R, I12L, and Y14V) when compared to PB1m6 (Fig. 2). In the previously reported cocrystal structure of PB1m6 and human PlxnB1 (13), Arg4 is shown to fit into a narrow pocket with its guanidinium group making several potential electrostatic interactions (Fig. 2*B*). In PB1m6A9, Arg4 is enigmatically mutated into a tyrosine which would not be able to take part in the majority of interactions the parental arginine residue is shown to make. All five analogs of PB1m6 show mutations in this position to an aromatic side chain (tyrosine or phenylalanine) (Fig. 2*A*). When modeling the PB1m6A9 mutations onto the previously solved cocrystal structure of PB1m6 (Fig. 2*B* and *SI Appendix*, Fig. S3), the benzene ring of Tyr4 on PB1m6A9 is in close proximity with Pro435 on PlxnB1 indicating a potential CH/π interaction (22). The parental Val5 and Ile12 residues, which point toward a hydrophobic patch on PlxnB1, are converted to isoleucine and leucine, respectively, in PB1m6A9 which can take part in the same interactions. Ala6 and Glu11 on the parental peptide are quite clearly solvent-exposed, and mutations to either side chain to glycine or alanine, respectively, show no major impact on binding affinity (*SI Appendix*, Fig. S4). However, Ala6 shows preference among PB1m6 analogs to be mutated to an acidic residue (Fig. 2*A*), suggesting a positive role for this mutation. Results from the PB1m6A9 model show this negatively charged A6E mutation hydrogen bonding with the mutated Arg11 guanidinium group which may form a potential salt bridge to further stabilize the β-hairpin structure of this peptide family (*SI Appendix*, Fig. S3). Tyr14 in the parental peptide is also an expendable side chain, and this position is mutated into a valine in PB1m6A9 which may simply be a neutral mutation. Also of importance is the conservation of residues 7 through 10, notably Arg7 and Trp8, which show marked decreases in affinity when mutated to alanines (*SI Appendix*, Fig. S4). Taken together, the mutational patterns show that the diversity in the library design allowed for the emergence of multiple beneficial mutations while retaining the binding mode of the parent peptide. Although our modeling efforts gave hints as to how these mutations are beneficial for increased affinity to PlxnB1, X-ray cocrystallography of PB1m6A9 with human and mouse PlxnB1 will be necessary to more confidently determine the positive contributions of these six mutations.

Homodimeric PB1d6A9 Peptides Show High Affinity and Cellular Activity In Vitro. Although PB1m6A9 exhibited high affinity to mPlxnB1, we speculated that it still lacked the potency to be tested in animal model studies. Therefore, we chose to synthesize homodimers of PB1m6A9 to improve its binding affinity against PlxnB1. We have previously reported that homodimerization of PB1m6 resulted in up to nearly 300-fold improvements in binding affinity as well as improvements in inhibiting the Sema4D-hPlxnB1 interaction on cells (23). To this end, we chemically synthesized the dimer of PB1m6A9 (PB1*d*6A9) in order to benefit from the same enhancements seen in the parent peptide, PB1m6 (Fig. 3*A* and *SI Appendix*, Figs. S5 and S6). As anticipated, SPR analysis of PB1*d*6A9 against mouse PlxnB1 showed similar enhancements to those previously seen with PB1m6, with an ∼220-fold improvement in K_D from 44 to 0.2 nM resulting from a 22-fold increase in association rate and a 10-fold decrease in dissociation rate (Fig. 3*A*).

With subnanomolar-binding affinity achieved against mPlxnB1, we examined PB1*d*6A9 treatment on mouse primary osteoblast differentiation where calcified nodules were visualized via alizarin red S staining (11). In the presence of 10 μg/mL mouse Sema4D-Fc fusion protein in the cell culture media, minimal bone formation was observed in vehicle-treated osteoblasts compared with a control sample (without Sema4D-Fc; Fig. 3*B*). In turn, the addition of PB1*d*6A9 in the presence of Sema4D-Fc showed dose-dependent increases in bone formation, and, strikingly, levels of bone formation were markedly higher than those of the control sample. This suggests that PB1*d*6A9 is not only an inhibitor of the Sema4D-mPlxnB1 interaction on the osteoblasts, but also a potent accelerator of osteoblastogenesis which is apparent by the dramatically enhanced progression of bone nodule formation in PB1*d*6A9-treated osteoblasts compared to the control osteoblasts. Consistent with these results, the expression of *Col1a1*, *Alpl*, and *Bglap*, all of which are involved in osteoblastic bone formation, were enhanced in PB1*d*6A9-treated osteoblasts even in the presence of Sema4D-Fc or compared to the vehicle control (Fig. 3*C*). In all instances, at maximal levels of peptide concentration (5 μM) the dimer peptide repeatedly showed higher levels of osteoblastogenesis. These observations suggest that the dimeric binding of PB1*d*6A9 on osteoblast surface mPlxnB1 molecules is capable of inducing a higher degree of osteoblastogenesis compared to standard cell culture conditions (i.e., in the absence of exogenously added Sema4D).

The Dimeric Peptides Induce Anabolic Effects In Vivo. With the potent osteogenic properties confirmed with PB1*d*6A9, we then proceeded to evaluate the PlxnB1-inhibitory mechanism of PB1*d*6A9 in vivo. In addition, while there are various approaches to improve pharmacokinetic (PK) properties of peptides, in this study we chose lipidation as a simple and relatively general method to improve peptide PK without further structure activity

A

ID	Sequence																Kinetics and affinity for mouse-PlxnB1 (human-PlxnB1)		
		1	2	3	4	5	6	7	8	9	10	11	12	13	14	15	16		k_a ($M^{-1}s^{-1}$)	k_d (s^{-1})	K_D (nM)
PB1m6	ClAc-	dw	R	P	R	V	A	R	W	T	G	Q	I	I	Y	C	S	-NH2	N.D. (7.8E+6)	N.D. (2.2E-2)	N.D. (2.8)
PB1m6A2				W	F	Y	D					T	F	Y	V		G		9.5E+5	5.6E-2	59
PB1m6A3			L	G	Y	I						T	V	V	K		G		6.2E+4	1.4E-2	227
PB1m6A5			L	A	Y	I	E							V	R		G		7.3E+4	3.7E-2	507
PB1m6A7				A	F	I	E					R	L	V	V		G		2.5E+5	3.2E-2	126
PB1m6A9					Y	I	E					R	L		V		G		4.0E+5 (7.6E+6)	1.8E-2 (2.1E-3)	44 (0.28)

B

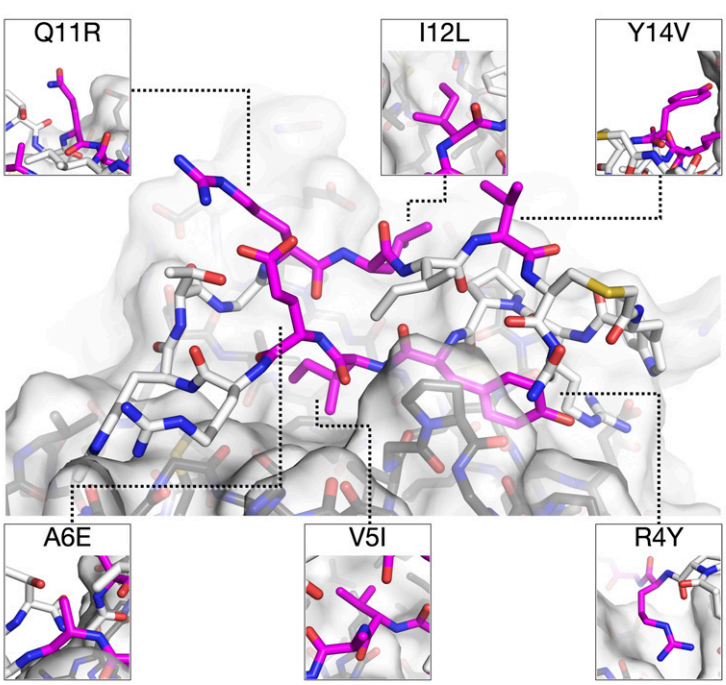

Fig. 2. PB1m6 analogs discovered in this study in comparison to the parent peptide. (*A*) Table comparing the sequences, binding kinetics, and affinities of peptides discovered in this selection with the parent sequence, PB1m6. (*B*) Model of PB1m6A9 (stick representation; red = oxygen, blue = nitrogen, yellow = sulfur) bound to mouse PlxnB1 (white transparent solvent-accessible surface over black stick representation) based on the crystal structure of PB1m6 bound to human PlxnB1 (Protein Data Bank ID: 5B4W), with small panels showing the corresponding mutated residue (magenta) contributions in the parent peptide, PB1m6.

relationship studies around PB1m6A9 (24). Thus, we proceeded to synthesize analogs of PB1m6A9 and PB1*d*6A9 with a C-terminal palmitoyl–lysine (*SI Appendix*, Figs. S5 and S6). Being that all peptides in our studies were discovered through RaPID selection with C-terminal glycine–serine linkers, it is well established that the peptide can be synthesized with various C-terminal modifications with only negligible effects on its intrinsic activity (13, 15).

We chose ovariectomized mice as a postmenopausal mouse model to compare the effect of once-weekly i.v. injections of the palmitoylated-monomeric (PB1m6A9-Pal), dimeric (PB1*d*6A9), and palmitoylated-dimeric (PB1*d*6A9-Pal) peptides over a 4-wk span (*SI Appendix*, Fig. S7*A*). Three-dimensional X-ray imaging of femurs by microcomputed tomography (μCT) revealed that the administration of a 5 μmol/kg dose of PB1*d*6A9 and PB1*d*6A9-Pal resulted in clear suppression of bone loss compared to vehicle controls, whereas 10 μmol/kg dose administration of PB1m6A9-Pal showed lesser effects on bone loss after 4 wk of treatment (Fig. 4*A*). Remarkably, 10 μmol/kg dose administration of PB1*d*6A9-Pal showed nearly complete suppression of bone loss, giving an observation of slightly denser bone than the sham control. In fact, the quantitative analyses of bone volume and thickness revealed that 10 μmol/kg dose treatment of PB1*d*6A9-Pal showed a statistically significant increase in trabecular and cortical bone indices at 4 wk compared with the sham control (Fig. 4*B* and *SI Appendix*, Fig. S7*B*). Histomorphometric analysis of tibiae also showed a significant increase in osteoblast and osteoid surfaces with enhanced calcein incorporation in mice treated with PB1*d*6A9-Pal (Fig. 4 *C* and *D* and *SI Appendix*, Fig. S7*C*). Furthermore, these mice also displayed reductions in the number of tartrate-resistant acid phosphatase (TRAP)-positive multinucleated cells and bone erosion, which were increased by estrogen deprivation (Fig. 4 *C* and *E* and *SI Appendix*, Fig. S7*C*). This additional anti-osteoclastogenic activity of PB1*d*6A9-Pal could be due to the suppression of the receptor activator of nuclear factor–κB-ligand (RANKL) expression and the ratio of RANKL/osteoprotegerin in bone (*SI Appendix*, Fig. S7*D*). Importantly, there were no statistically significant differences in serum biochemical parameters between the treatment groups and the control after 4 wk of the ovariectomy (*SI Appendix*, Table S2). These data suggest that PB1*d*6A9-Pal could be a novel anabolic agent to treat patients with bone loss by stimulating osteoblastic bone formation and inhibiting osteoclastic bone resorption through its unique PlxnB1-binding mechanism.

Discussion

With the continuing increase in global median age, the number of those impacted by osteoporosis is on the rise as well (25). Bone fractures stemming from osteoporosis lead to lower quality of life in those affected, and treatment combined with inability to work costs billions per year globally (1, 2, 25). Adult bone is established by a balance between osteoclastic bone resorption and osteoblastic bone formation, and current therapeutic treatment options for osteoporosis aim to restore bone density by either inhibiting resorption (antiresorptives) or by enhancing formation (anabolics) (6). Currently, antiresorptives such as bisphosphonates are the first-line treatment for osteoporosis. However, while these traditional therapeutics increase bone density, they are not able to

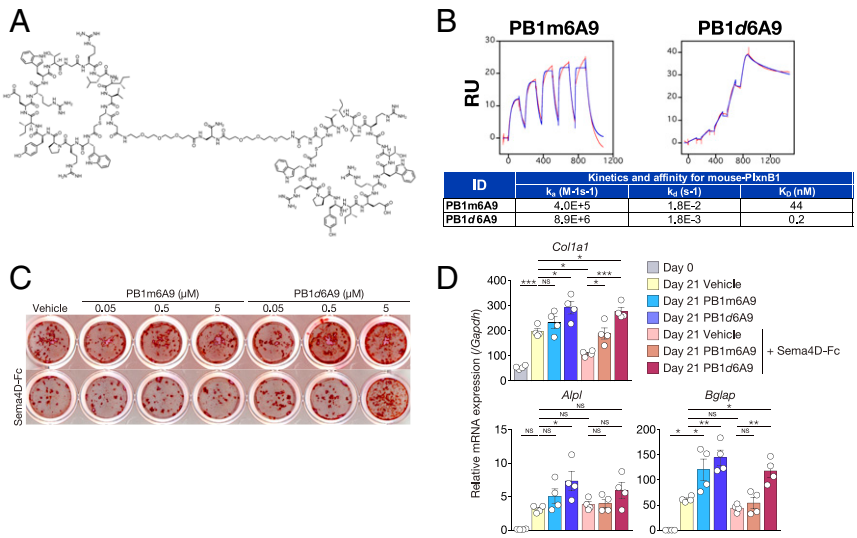

Fig. 3. Comparison of PB1m6A9 and its homodimer PB1*d*6A9, in surface plasmon resonance analysis and in vitro bone nodule formation. (*A*) Structural formula of PB1*d*6A9. (*B*) SPR sensorgrams, kinetics, and affinities for PB1m6A9 and PB1*d*6A9 against mouse PlexinB1. (*C*) Effects of PB1m6A9 and PB1*d*6A9 on bone nodule formation in primary calvarial cells via alizarin red S staining. (*D*) Effects of PB1m6A9 and PB1*d*6A9 with or without mouse Sema4D-Fc treatment on mRNA expressions of the genes implicated in osteoblastic bone formation. All data are presented as mean ± SEM $*P < 0.05$; $**P < 0.01$; $***P < 0.001$; NS, not significant; by one-way ANOVA and Tukey's post hoc test. Circles represent individual data points.

reverse microstructural deterioration which is an important component of bone integrity and preventing fractures (6). In contrast, anabolic agents are able to enhance bone formation without decreasing bone resorption and are able to restore bone volume and microstructure. At present, the only anabolic agents in the clinic are the peptides teriparatide, abaloparatide, and the monoclonal antibody romosozumab. Unfortunately, all three anabolics have relatively short maximum treatment durations due to risk of osteosarcoma for teriparatide and abaloparatide and decreasing efficacy past 1 y for romosozumab (7, 8). Here we report PB1*d*6A9-Pal which can potentially be another promising anabolic treatment option for osteoporosis. Importantly, PB1*d*6A9-Pal delivers its anabolic effects by engaging PlxnB1 directly on osteoblasts which sets it apart mechanistically from the aforementioned anabolics. The direct activity of this peptide was clearly demonstrated by inducing enhanced osteoblastogenesis in mouse primary osteoblast culture which also opens the possible application of this peptide as a chemically defined molecule for use in bone cell cultures (26). In vivo, the PB1*d*6A9-Pal peptide showed striking reversal of bone loss in ovariectomized mice with once-weekly injections.

Previous results have shown that the administration of an anti-Sema4D antibody can protect mice from ovariectomy-induced bone loss by activating bone formation (11). However, the therapeutic effect was a limited one because the prevention of bone loss tended to be partial, and the bone mass of antibody-treated animals did not exceed Sham controls. In addition, reports of bone-targeted delivery of siRNAs against *Sema4d* has also been demonstrated to show reversal of ovariectomy (OVX)-induced bone loss, albeit to a partial level (27). In contrast, bone mass of ovariectomized mice that received the optimal dose administration of PB1*d*6A9-Pal was indistinguishable from that of Sham controls (Fig. 4 *A* and *B*), indicating that it can completely reverse the bone loss phenotype caused by OVX. Moreover, the in vitro differentiation of osteoblasts was up-regulated by PB1*d*6A9 treatment even compared to non-Sema4D–treated controls (Fig. 3 *B* and *C*). We posit that this is due to the inhibition of baseline or "constitutive" antiosteoblastogenic signaling impinging on PlxnB1 in resting cells which may act as an intrinsic safeguard against spontaneous osteoblast differentiation. This is based on previous observations of a bimodal inhibition curve when the dimeric version of PB1m6 was tested in a cell collapse assay using hPlxnB1-expressing cells (23). Taken together with the solved cocrystal structure of PB1m6 and hPlxnB1, the first inhibitory maximum in the low nanomolar range likely represents signal inhibition via sequestration of cell surface hPlxnB1 molecules in nonfunctional outward facing dimer conformations. If a low baseline level of PlxnB1 dimers on resting precursor cells is playing a role in the suppression of differentiation, PB1*d*6A9 may liberate PlxnB1 from this signal-transducing dimer, in this case leading to the enhancement of bone formation. Further validation of this hypothesis and revealing the details of its mechanism await further studies.

Apart from the biological activities of the PB1m6A9 series, the novel selection methodology demonstrated in this work was able to tune the species specificity and increase the binding affinity of in vitro selected macrocyclic peptides for quick advancement to in vivo efficacy studies. Traditionally, optimization of therapeutic peptides requires several rounds of positional scans and analoging, requiring considerable time and cost for chemical synthesis, purification, and in vitro and in vivo evaluation. By taking advantage of the large diversity of the RaPID system ($>10^{12}$) and generating an mRNA library of $\sim 10^{11}$ analogs of PB1m6 in "one-pot" (Fig. 1) we were able to generate the human–mouse PlexinB1 cross-reactive analog PB1m6A9 within just five rounds of selection (*SI Appendix*, Fig. S1). While the parent peptide PB1m6 showed no binding toward mPlxnB1, PB1m6A9 showed a K_D of 44 nM and serendipitously also showed over 10-fold improved affinity toward hPlxnB1 at 0.2 nM K_D (Fig. 2*A* and *SI Appendix*, Fig. S2). Comparison of the parental peptide-binding mode to PB1m6A9 reveals mutations that would be difficult to conceive through rational design or single-point mutations (Fig. 2*B*), and follow-up cocrystallography efforts with human and mouse PlxnB1 will be of high interest to explain the contributions of these mutations. The ability of this motif to now bind the mouse homolog opened up the door for validation of its therapeutic activity in vivo. Applying previously reported strategies for cyclic peptide homodimerization (23) and lipidation (24) via an added palmitoyl–lysine (*SI Appendix*, Figs. S5 and S6), we were able to systematically improve binding affinity and in vivo

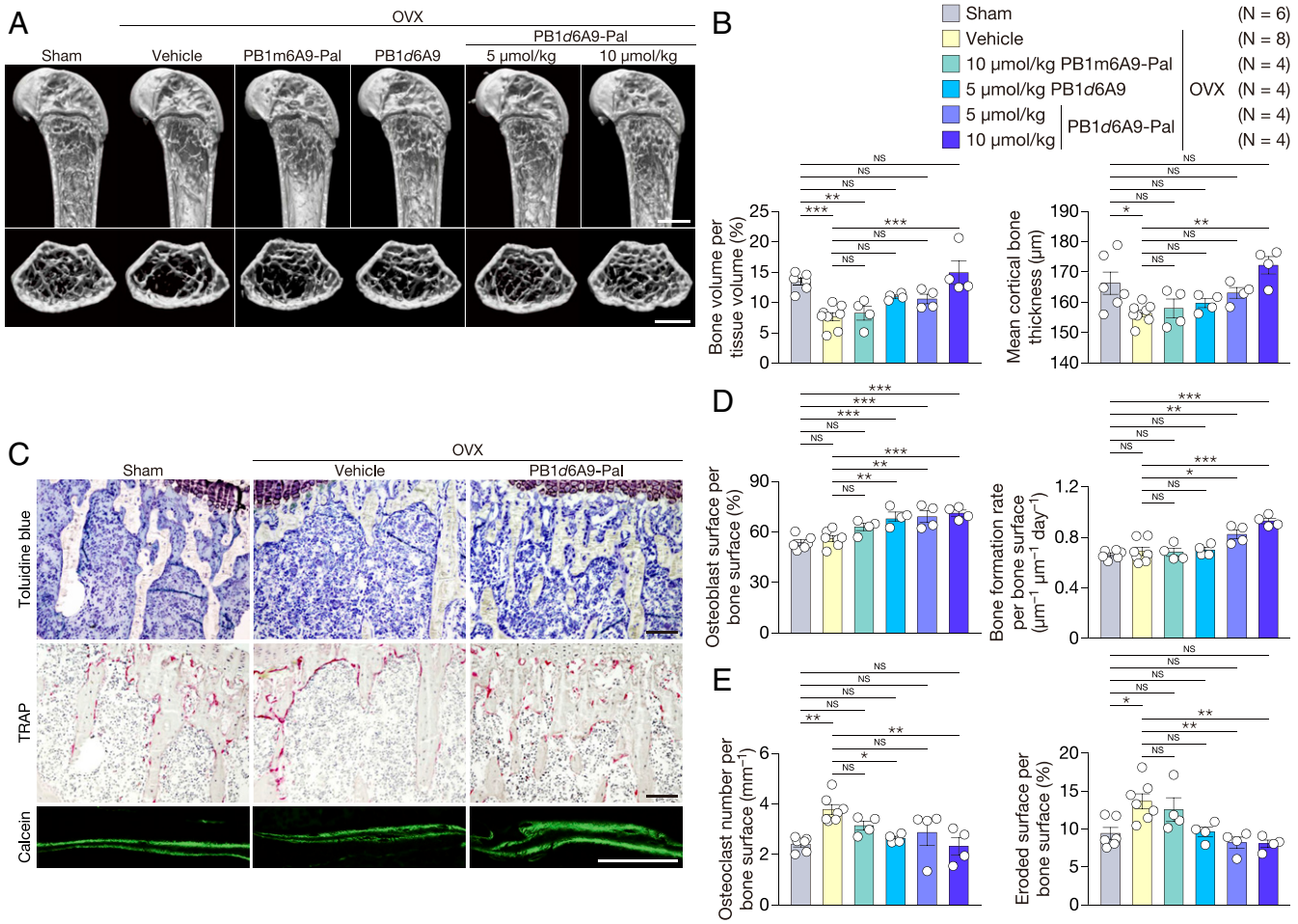

Fig. 4. In vivo efficacy of PB1m6A9 analogs. (*A* and *B*) Representative μCT images (*A*) and μCT analysis of distal femurs (*B*) in Sham or OVX mice with PB1m6A9Pal, PB1*d*6A9, PB1*d*6A9-Pal, or vehicle treatment. Circles represent individual data points. (*C*–*E*) Histological images of proximal tibiae (*C*), osteoblastic (*D*), and osteoclastic (*E*) parameters in bone morphometric analysis of tibiae in sham-operated or ovariectomized mice with PB1m6A9-Pal, PB1*d*6A9, PB1*d*6A9-Pal, or vehicle treatment. All data are presented as mean ± SEM $*P < 0.05$; $**P < 0.01$; $***P < 0.001$; NS, not significant; by one-way ANOVA and Tukey's post hoc test. Circles represent individual data points.

efficacy resulting in PB1*d*6A9-Pal which was able to fully ameliorate the bone loss resulting from OVX (Fig. 4 and *SI Appendix*, Fig. S7).

While the dimeric palmitoylated macrocyclic peptide PB1*d*6A9-Pal presented in this study showed remarkable results in reversing the advancement of osteoporosis-related bone loss with just once-weekly administrations in the mouse model, there are limitations when comparing rates of osteogenesis between human and mouse (28). Future studies in nonhuman primate models will be necessary to better predict efficacy in humans (29). In nonhuman primates commonly used as models for postmenopausal osteoporosis, the homology of the PB1m6-peptide family binding domain is much higher (97–98%) than for the mouse homolog (88%); therefore, affinities closer to what was observed for human PlxnB1 can be anticipated (>150-fold lower K_D compared to mouse PlxnB1). Follow-up optimizations focused on improving the pharmacokinetics of the parent peptide while retaining binding affinity will be pursued as well as investigating drug delivery methods in an effort to further increase the in vivo potency of these peptides.

Materials and Methods

Synthesis of PB1m6-Based mRNA Library. All oligonucleotides used in this study were purchased from Eurofins, and the sequences are listed in *SI Appendix*, Table S1. DNA templates for the mRNA library were prepared via assembly PCR (95 °C, 1 min; 65 °C, 1 min; 72 °C, 1 min; repeated five cycles) by pooling the 49 FWmP6 oligonucleotides which each encode a sublibrary along with the reverse primer CGS3an13.R39. The FWmP6 pool was mixed with CGS3an13.R39 at a ratio of 1:3 to ensure every FWmP6 template would be extended. Assembly PCR products then underwent 15 cycles of standard PCR amplification (94 °C, 40 s; 50 °C, 40 s; 72 °C, 40 s) using T7g10M.F48 and CGS3an13.R39. The PCR product was then purified by phenol–chloroform extraction followed by ethanol precipitation. The purified DNA library was then in vitro transcribed via T7 Polymerase and gel-purified using a 5% urea–polyacrylamide gel electrophoresis (PAGE) gel; quality was verified on an 8% urea–PAGE gel. After being adjusted to 50 μM the mRNA library was stored at −20 °C until further use.

Aminoacylation of transfer RNA$^{fMET}_{CAU}$. An equal mixture of in-house synthesized flexizyme and formyl–methionine initiator transfer RNA (tRNA$^{fMET}_{CAU}$) was prepared to a final concentration of 31.25 μM, in 62.5 mM Hepes–KOH (pH 7.5) with 750 mM $MgCl_2$. *N*-chloroacetyl–D-tryptophan cyanomethyl ester was added to a final concentration of 5 mM, and the reaction was incubated on ice for 1.5 h. This was followed by precipitation with 70% ethanol/ 0.1 M sodium acetate mixture (pH 5.2) and recovery by centrifugation at ∼15,000 × *g* for 15 min. The resulting amino acylated tRNAs (ClAc-D-Trp-tRNA$^{fMET}_{CAU}$) obtained were kept at −80 °C until further use.

RaPID Selection against mPlxnB1. RaPID selection against mPlxnB1 was performed as previously described by Matsunaga et al. (13), with the exception that avitag-biotinylated ectodomain of hPlxnB1 was replaced with the avitag-biotinylated ectodomain of mPlxnB1, and the starting mRNA library used was a PB1m6-based mRNA library. Briefly, after ligation of the PB1m6-based mRNA library to a puromycin linker by T4 RNA ligase at 25 °C for

30 min, the mRNA library was precipitated with ethanol/NaCl and resuspended in water. Translation was performed via FIT system translation (30) without methionine at 150-μL scale at 37 °C for 30 min, together with the initiator ClAc-D-Trp-tRNA$^{fMET}_{CAU}$ at a final concentration of 50 μM. The reaction was subsequently incubated for 12 min at 25 °C to allow fusion of the mRNA and peptide, followed by addition of EDTA to 16.7 μM and further incubation for 30 min at 37 °C to release the mRNA-peptide fusion molecules from the ribosome. Reverse transcription was performed using Moloney Murine Leukemia Virus reverse transcriptase (RNase H-) (Promega) with the CGS3an13.R39 primer at 42 °C for 1 h. The products from reverse transcription were desalted through a resin of engorged sephadex-G25 (GE Healthcare) in Tris-buffered saline 0.05% Tween20 (TBST) buffer by centrifugation at 900 × *g* for 1 min. An equal volume of blocking buffer (TBST + 0.2% acetylated BSA [Life Technologies]) was added to the collected flow-through, and 0.5 μL of the mixture was transferred to 500 μL of water as input for latter qPCR analysis. In parallel, beads for positive selection were prepared by treating 150 μL of Dynabeads M-280 Streptavidin (Thermo Fisher Scientific) with 75 μL of 4-μM avitag-biotinylated mouse PlexinB1 extracellular domain at 4 °C for 15 min, followed by a further 15 min at 4 °C with free biotin (final concentration 25 μM) to block unliganded streptavidin. After protein binding, beads were washed with TBST (50 mM Tris, 150 mM NaCl, 0.05% Tween-20) three times prior to selection. The prepared beads then have the buffer replaced with the reverse-transcribed peptide–mRNA fusion library and incubated at 4 °C for 30 min. After three washes with 150 μL of cold TBST, mRNA-peptide fusion molecules were eluted from beads with 400 μL PCR Mix (with 0.25 μM T7g10M.F48 and 0.25 μM CGS3an13.R39) at 95 °C for 5 min. One microliter of the recovered DNA, as well as the previously diluted input sample, were quantified using real-time PCR (Roche Light Cycler 2.0), with SYBR Green I detection. A series of 10-fold dilutions of reverse-transcribed initial mRNA library were used as standards. PCR of the recovered DNA was amplified for two cycles more than the cq values obtained from qPCR. Once amplification was confirmed through agarose gel electrophoresis, the sample was phenol/choloroform/isoamyl alcohol-extracted, ethanol-precipitated, resuspended in 50 mM KCl, and stored at −20 °C until transcription for the subsequent round of selection.

For round 2 to 5, DNA templates from the previous round were first transcribed at 37 °C overnight. The obtained mRNA templates were adjusted to 10 μM in water based on measurements on NanoDrop 2000c Spectrophotometer (Thermo Scientific). Puromycin ligation and subsequent treatments were performed identically to round 1, with the exception that the reactions were scaled down 30-fold. In addition, prior to the positive selection, the products from reverse transcription are first treated three times with 5 μL of counterselection beads (an equal mixture of biotin-bound and nonbiotin-bound streptavidin Dynabeads) at 4 °C for 15 min to eliminate bead-binding peptides. The supernatant from the final negative selection was then used for positive selection with 5 μL of mPlexinB1-bound beads. Elution from negative selection beads was performed with 20 μL of PCR mix for use in qPCR, and 100 μL of PCR mix was used for beads from positive selections.

Peptide Synthesis. All monomeric and homodimeric peptides were synthesized as previously described by Bashiruddin et al. (23). PB1m6A9-Pal and PB1*d*6A9-Pal were synthesized in the same manner as PB1m6A9 and PB1*d*6A9, with the exception that Fmoc–*N*-ε-palmitoyl-L-lysine was the first Fmoc–amino acid to be coupled to the resin for solid-phase peptide synthesis.

Surface Plasmon Resonance. Surface plasmon resonance measurements were performed on a Biacore T200 machine (GE Healthcare Life Sciences). Avitagged ectodomain of mPlxnB1 was immobilized onto a CAP sensor chip covered with Streptavidin-coupled oligo-SA (biotin-CAPture reagent). Filter-sterilized TBST containing 0.1% DMSO was used as running buffer and for dilution of samples (13). After an initial regeneration step with 6 M guanidine–HCl, 250 mM NaOH for 120 s at 20 μL/min, two lanes of the CAP sensor chip were coupled with oligo-SA for 300 s at 2 μL/min. A 100 nM concentration of the biotinylated ectodomain of mouse PlxnB1 was then immobilized on the second lane at 2 μL/min for 600 s. Five concentrations (1, 10, 100, 500, and 1,000 nM) of each peptide were analyzed in the initial measurement, using single-cycle kinetics. Further refinement was performed with peptides at concentrations ∼10 times the initial K_D with four twofold dilutions. Analyses against human PlxnB1 were performed as previously described by Bashiruddin et al. (23).

Modeling of the PB1m6A9-mPlexinB1 Complex. The Macromodel module v10 within Schrödinger, Inc. was used for conformational calculations of the PB1m6A9-mPlexinB1 complex. The structure was built within Maestro version 11.9.011. based on previously reported structures (PB1m6-hPlexinB1 complex [PDB ID: 5B4W]). Both structures were superimposed, hPlexinB1 was deleted, and the PB1m6 sequence was manually mutated to PB1m6A9. The OPLS3e forcefield was used, and the conformational search was conducted in water as solvent. Extended cutoffs were used to model interactions. A substructure function was set around 5 Å of PB1m6A9 for atoms to move freely, the 5- to 10-Å range was set to be constrained under a force constant of 200, and the 10- to 15-Å range was frozen. A low-mode sampling approach was used to generate conformers with intermediate torsional sampling. A total of 100 conformers were generated. All conformers were subjected to further minimization using the Powell–Reeves conjugate gradient method for a maximum of 2,500 steps, and structures within 21 kJ/mol of the lowest energy were saved for analysis. The nine lowest-energy structures from each calculation are shown in *SI Appendix*, Fig. S3, and a representative conformation is shown in Fig. 2*B*.

Cell Culture. Calvarial cells were isolated from the calvarial bone of newborn C57BL/6J mice by enzymatic digestion in α-Minimum Essential Medium (MEM) with 0.1% collagenase and 0.2% dispase and were cultured with α-MEM with 10% fetal bovine serum. After 2 d, cells were reseeded (1×10^4 cells per cm^2) and cultured with osteogenic medium (50 μM ascorbic acid 2-phosphate sesquimagnesium salt, 5 mM β-glycerophosphate, and 10 nM dexamethasone) with or without 0.05, 0.5, and 5 μM PB1m6A9, PB1*d*6A9, or vehicle. Culture medium was changed every third day. After 21 d, bone nodule formation was assessed by alizarin red S staining (Sigma).

qPCR. Total RNA was isolated using Direct-zol RNA MiniPrep Kit (Zymo Research) according to the manufacturer's instructions. First-strand cDNAs were synthesized using SuperScript IV VILO Master Mix (Thermo Fisher Scientific). qPCR analysis was performed with the CFX384 Touch Real-Time PCR Detection System (Bio-Rad Laboratories) using Probe qPCR Mix (TaKaRa) and Probe qPCR assays (Integrated DNA Technologies). Bone fraction was isolated from the femur by centrifugation.

Mice and Bone Analysis. C57BL/6J mice were purchased from CLEA Japan and maintained under specific-pathogen–free conditions. All animal experiments were approved by the Institutional Animal Care and Use Committee of Tokyo Medical and Dental University. Bone tissues were fixed with 70% ethanol, and μCT scanning was performed using a ScanXmate-A100S Scanner (Comscantecno). Three-dimensional microstructural image data were reconstructed, and structural indices were calculated using TRI/3D-BON software (RATOC Systems). For the analysis of osteoblasts and osteoclasts, the undecalcified tibiae were embedded in glycol methacrylate, sectioned (5 μm), and stained with toluidine blue and TRAP, respectively. Images were taken using a light microscope (Axio Imager 2, Zeiss), and all histological analyses were performed using WinROOF 2013 software (Mitani).

Data Availability. All study data are included in the article and supporting information.

ACKNOWLEDGMENTS. This work was supported in part by Japan Agency for Medical Research and Development, Platform Project for Supporting Drug Discovery and Life Science Research (Basis for Supporting Innovative Drug Discovery and Life Science Research) under JP19am0101090 and 19am0101075 (to H.S. and J.T., respectively); Advanced Research and Development Programs for Medical Innovation under JP19gm0810003 and JP19gm6110027 (to T.N. and M.H., respectively); Grants-in-Aid for Scientific Research (B) (to T.N.) and Challenging Research (Exploratory) (to M.H.) from the Japan Society for the Promotion of Science; and grants from Takeda Science Foundation, Naito Foundation, Mitsui Life Social Welfare Foundation, Daiichi Sankyo Foundation, and Secom Science and Technology Foundation (to T.N.).

1. J. E. Compston, M. R. McClung, W. D. Leslie, Osteoporosis. *Lancet* **393**, 364–376 (2019).
2. K. N. Tu *et al*., Osteoporosis: A review of treatment options. *P&T* **43**, 92–104 (2018).
3. F. Cosman, J. W. Nieves, D. W. Dempster, Treatment sequence matters: Anabolic and antiresorptive therapy for osteoporosis. *J. Bone Miner. Res.* **32**, 198–202 (2017).
4. K. G. Saag *et al*., Romosozumab or alendronate for fracture prevention in women with osteoporosis. *N. Engl. J. Med.* **377**, 1417–1427 (2017).
5. D. L. Kendler *et al*., Effects of teriparatide and risedronate on new fractures in post-menopausal women with severe osteoporosis (VERO): A multicentre, double-blind, double-dummy, randomised controlled trial. *Lancet* **391**, 230–240 (2018).

6. E. Seeman, T. J. Martin, Antiresorptive and anabolic agents in the prevention and reversal of bone fragility. *Nat. Rev. Rheumatol.* **15**, 225–236 (2019).
7. A. H. Tashjian Jr, B. A. Chabner, Commentary on clinical safety of recombinant human parathyroid hormone 1-34 in the treatment of osteoporosis in men and postmenopausal women. *J. Bone Miner. Res.* **17**, 1151–1161 (2002).
8. M. R. McClung, Romosozumab for the treatment of osteoporosis. *Osteoporos. Sarcopenia* **4**, 11–15 (2018).
9. N. A. Sims, T. J. Martin, Osteoclasts provide coupling signals to osteoblast lineage cells through multiple mechanisms. *Annu. Rev. Physiol.* **82**, 507–529 (2020).
10. T. Worzfeld, S. Offermanns, Semaphorins and plexins as therapeutic targets. *Nat. Rev. Drug Discov.* **13**, 603–621 (2014).
11. T. Negishi-Koga *et al*., Suppression of bone formation by osteoclastic expression of semaphorin 4D. *Nat. Med.* **17**, 1473–1480 (2011).
12. C. Tsiamantas, M. E. Otero-Ramirez, H. Suga, Discovery of functional macrocyclic peptides by means of the RaPID system. *Methods Mol. Biol.* **2001**, 299–315 (2019).
13. Y. Matsunaga, N. K. Bashiruddin, Y. Kitago, J. Takagi, H. Suga, Allosteric inhibition of a semaphorin 4D receptor plexin B1 by a high-affinity macrocyclic peptide. *Cell Chem. Biol.* **23**, 1341–1350 (2016).
14. Y. Hayashi, J. Morimoto, H. Suga, In vitro selection of anti-Akt2 thioether-macrocyclic peptides leading to isoform-selective inhibitors. *ACS Chem. Biol.* **7**, 607–613 (2012).
15. K. Ito *et al*., Artificial human Met agonists based on macrocycle scaffolds. *Nat. Commun.* **6**, 6373 (2015).
16. A. Kawamura *et al*., Highly selective inhibition of histone demethylases by de novo macrocyclic peptides. *Nat. Commun.* **8**, 14773 (2017).
17. S. A. K. Jongkees *et al*., Rapid discovery of potent and selective glycosidase-inhibiting de novo peptides. *Cell Chem. Biol.* **24**, 381–390 (2017).
18. M. Nawatha *et al*., De novo macrocyclic peptides that specifically modulate Lys48-linked ubiquitin chains. *Nat. Chem.* **11**, 644–652 (2019).
19. J. M. Rogers, T. Passioura, H. Suga, Nonproteinogenic deep mutational scanning of linear and cyclic peptides. *Proc. Natl. Acad. Sci. U.S.A.* **115**, 10959–10964 (2018).
20. M. S. Packer, D. R. Liu, Methods for the directed evolution of proteins. *Nat. Rev. Genet.* **16**, 379–394 (2015).
21. C. D. Wassman, P. Y. Tam, R. H. Lathrop, G. A. Weiss, Predicting oligonucleotide-directed mutagenesis failures in protein engineering. *Nucleic Acids Res.* **32**, 6407–6413 (2004).
22. N. J. Zondlo, Aromatic-proline interactions: Electronically tunable CH/π interactions. *Acc. Chem. Res.* **46**, 1039–1049 (2013).
23. N. K. Bashiruddin, Y. Matsunaga, M. Nagano, J. Takagi, H. Suga, Facile synthesis of dimeric thioether-macrocyclic peptides with antibody-like affinity against plexin-B1. *Bioconjug. Chem.* **29**, 1847–1851 (2018).
24. L. Zhang, G. Bulaj, Converting peptides into drug leads by lipidation. *Curr. Med. Chem.* **19**, 1602–1618 (2012).
25. M. A. Clynes *et al*., The epidemiology of osteoporosis. *Br. Med. Bull.* **133**, 105–117 (2020).
26. S. Kargozar *et al*., Bone tissue engineering using human cells: A comprehensive review on recent trends, current prospects, and recommendations. *Appl. Sci.* **9**, 174 (2019).
27. Y. Zhang, L. Wei, R. J. Miron, B. Shi, Z. Bian, Bone scaffolds loaded with siRNA-Semaphorin4d for the treatment of osteoporosis related bone defects. *Sci. Rep.* **6**, 26925 (2016).
28. R. L. Jilka, The relevance of mouse models for investigating age-related bone loss in humans. *J. Gerontol. A Biol. Sci. Med. Sci.* **68**, 1209–1217 (2013).
29. S. Y. Smith, A. Varela, J. Jolette, "Nonhuman primate models of osteoporosis" in *Osteoporosis Research*, G. Duque, K. Watanabe, Eds. (Springer London, 2011), pp. 135–157.
30. Y. Goto, T. Katoh, H. Suga, Flexizymes for genetic code reprogramming. *Nat. Protoc.* **6**, 779–790 (2011).